Materials Today Communications 37 (2023) 106917

Contents lists available at ScienceDirect

Materials Today Communications

journal homepage: www.elsevier.com/locate/mtcomm

^{57}Fe Mössbauer, optical and structural properties with ligand field effects of borosilicate glass doped with iron oxide

H.Y. Morshidy [a,*], Essam A. Elkelany [b], Kareem T. Abul-Nasr [c], A. Samir [d], H.H. El-Bahnasawy [e], Moukhtar A. Hassan [e,*]

[a] Research & Studies Center, Midocean University, Moroni 6063, Comoros
[b] Basic Science Department, Faculty of Engineering, Sinai University, Al-Arish 45511, Egypt
[c] Physics Department, Faculty of Science, Port-Said University, Port-Said 42521, Egypt
[d] Basic Science Department, Faculty of Engineering at Shoubra, Benha University, 11629, Egypt
[e] Physics Department, Faculty of Science, Al-Azhar University, Cairo 11884, Egypt

ARTICLE INFO

Keywords:
Borosilicate glass
Iron oxide
Ligand field
Optical features
Mössbauer spectra

ABSTRACT

Here, an investigation of borosilicate glass doped with iron oxide and prepared by classical melt-quenching method. The internal macrostructure, optical absorbance, ligand field parameters, and Mössbauer spectra were studied. The density increased with increasing SiO_2 content, while Fourier-transform infrared (FTIR) analysis reported that BO_4 and SiO_4 content increase with a decrease in NBO content. Optical electronic transitions through wavelength (402–948 nm) confirmed the existence of Fe^{3+} state, while the Fe^{2+} is not observed in optical absorbance because of its inane electronic transition at 2222 nm. The electronic transitions at (402, 452, 513, 602, and 701 nm) are assigned to Fe^{3+} in tetrahedral coordination (FeO_4), while the electronic transitions at (795 and 948 nm) are related to Fe^{3+} in octahedral coordination (FeO_6). Astonishingly, the ligand field parameters of Fe ions were studied. The crystal field splitting exhibits increasing values, while Racah parameters exhibit decreasing values. Moreover, nephelauxetic parameters reflect the propensity of the bonding nature between the Fe cations and their ligands towards a higher covalent nature with SiO_2 additives. Further, a scant decrease in the optical band gap was explained based on the mixed former effect. Moreover, non-linear refractive indices augment with SiO_2 addition. The decrease in the optical gap energy justified such a trend. Bewitchingly, Mössbauer spectra reported the existence of Fe^{3+} ions with isomer shift (0.285–0.314) mm s^{-1} in tetrahedral sites, while Fe^{3+} ions with isomer shift (0.339–0.425) mm s^{-1} in octahedral sites, agreeing with optical data. Surprisingly, Fe^{2+} ions with isomer shift at about 0.905 mm s^{-1} in tetrahedral sites was observed. The observed decrease in isomer shift of all phases is due to the decrease in electronegativity of formers. Furthermore, the decrease in quadrable splitting is attributed to the decline in the polarization power of the glass former cations with SiO_2 addition.

1. Introduction

Recently, the industry has focused on technological applications demanding tunable optical characteristics with low energy consumption [1]. In this context, oxide glasses offer some advantages that are especially suitable for exploring new functional materials [2]. Due to the constancy during device working, high refractive index, thermal stability, chemical resistance, high transparency, good solubility of dopants, and melting at low temperatures, boron oxide is one of the best glass formers [3]. The importance of boron oxide manifests from its distinct characteristics besides its applicability in a plethora of applications in the optics sector. In addition, silicon oxide has a similar weight of importance in glass science due to its high chemical and thermal stability [1]. However, embedding silicon oxide, as a former oxide, to the borate glass network establishes a new type of glass former, borosilicate glass (BS). The boron oxide combined with silicon oxide made a prodigious glass borosilicate network (BS) that has a set of characterized building units (BO_3, BO_4 and SiO_4), rendering them a good host for accommodating large-scale dopants [4,5]. Borosilicate glass is the most familiar glass network. Its significance is that it has the

* Corresponding authors.
E-mail addresses: hesham_yahia25@yahoo.com (H.Y. Morshidy), m.a.hassan@azhar.edu.eg (M.A. Hassan).

https://doi.org/10.1016/j.mtcomm.2023.106917
Received 16 July 2023; Received in revised form 12 August 2023; Accepted 17 August 2023
Available online 22 August 2023

combined features of both former oxides, and consequently, this network is exploited in large-scale applications [2,6]. Borosilicate glass exhibits high chemical durability and mechanical resistance. It is used for various applications, including optical communication, glass-to-metal sealing, ion exchange materials, durable glass containers, and nuclear waste immobilization [2,7]. Borosilicate glass is easy to prepare, cheap cost preparation, and high mass production of its products [7].

Furthermore, adding alkali oxides as modifier oxides to the borosilicate host was reported to enhance the physicochemical of the glass samples. A plethora of charming properties, including high transparency, high conductivity, high stability, high gloss and shine, and low melting temperature, were obtained as the lithium oxide (Li_2O) is added as a modifier alkali oxide. Lithium oxide is an unique alkali oxide that characterizes by readily solubility and minimizes the bubble-free [7,8]. Furthermore, structural modifications are established by lithium ions, including the conversion from BO_3 units to BO_4 units and contrariwise [9], and the interstitial filling [10]. The relationship between composition-properties of B_2O_3-SiO_2- Li_2O glass system was studied in Refs. [11,12]. Recently, Sugawara et al. [10] studied the effect of composition change in $Li_2B_4O_7$ glass. They evaluated the changes resulting from converting BO_3 into BO_4 units in case of the existence of SiO_4 units.

Borosilicate glass containing transition metal ions is the subject of interest due to its potential applications in luminescent materials [2,7]. Particularly iron oxide (Fe_2O_3) is one of the great interest oxides. Iron oxide exists in various oxidation states (divalent, trivalent, …) with different symmetry sites (octahedral, tetrahedral, …) [13,14]. In glass material, the co-existence of two valence states of iron ions (Fe^{2+} and Fe^{3+}) is a common condition in borosilicate glasses [9,15]. Iron oxide is a crucial ingredient in colored glasses. The oxidation state of iron ions in glasses relies on chemical composition and melting process. While the symmetry of these ions depends on the surrounding ligand field of iron ions [13,14]. Due to its electronic structure and optical transitions, iron oxide is exploited to give the glasses brown or honey color [16,17]. Ligand field theory explains the originality of such color and its variation in the glasses containing iron ions. Besides, a theory studies the structural/optical changes of the transition metal ions (here, iron ions) in optically active glass material. According to our large-scale knowledge in this field, the first paper which reported the ligand field parameters of iron ions embedded in glass was published (in 2020) by Elkelany et al. [17]. They reported the structural/optical modifications of iron ions in borate glass using ligand field theory. In this regard, use of ligand field theory to investigate the structural/optical relationships in glass materials is needed and is considered a hot point in optics field. There are no reported studies on the utilization of ligand field theory to investigate the structural/optical characteristics of iron ions embedded in lithium-borosilicate glasses. From this perspective, the current work aims to investigate the impact of progressive silicon addition on the structural/optical features of lithium-borosilicate glass using the ligand field theory of iron ions, with a decent investigation of Mössbauer spectra. The present study aims to present a specific structural/optical perspective of borosilicate glasses containing iron ions as a developed functional material which has a promising viability in optical sector.

2. Experimental methodology

2.1. Samples preparation

Four glass samples with a formula of [(70-x) B_2O_3 - x SiO_2 - 24 Li_2O - 6 Fe_2O_3] where (x = 0, 20, 40, and 60 mol%) were successfully synthesized by classical melt quenching method. The chemical composition of the prepared samples and the samples' code were labelled in Table 1. Preliminary, high-purity raw materials are Li_2CO_3, Fe_2O_3, H_3BO_3 and SiO_2 were purchased from Sigma-Aldrich. To ensure adequate high homogeneity, the appropriate stoichiometric quantities of the precursors were gently weighted utilizing an electric single pan balance with a precision (0.001) g sensitivity. Then, the powders were thoroughly mixed in a mortar to guarantee a good mixing process. The obtained batches were melted in a furnace. The temperature increased from room temperature up to the melting point, with heating rate 30 ℃/min, to ensure the best volatilization of gasses and remove the bubble-free. The melting temperature of samples was at 1100–1200 °C for 40 min, according to each composition. The porcelain crucibles were continuously stirred to ensure adequate mixture homogeneity of all ingredients. Finally, the molten glass was quickly poured and quenched between two clean and polished plates at room temperature, to produce uniform glass samples of thickness is about ~ 0.5 mm. The glass samples were transparent and bubble-free, and with reddish-brown color. Complementary measurements (density, optical, …) were carried out on the bulk samples after polishing. The other part of these samples was milled in an agate mortar to get a fine powder for other planned measurements such as FT-IR and Mossbauer.

Table 1
The chemical composition of all glass samples.

Sample code (mol%)	SiO_2	B_2O_3	Li_2O	Fe_2O_3
0 Si	0	70	24	6
20 Si	20	50	24	6
40 Si	40	30	24	6
60 Si	60	10	24	6

2.2. Samples characterization

To investigate the impactive SiO_2 modifications on some structural and optical properties of the lithium iron-based borosilicate glass. The mass density of samples was carried out using Archimedes' principle in the case of the immersed sample. The toluene-static fluid was exploited and combined with a sensitive micro-single balance. By measuring five trials for each sample under the same conditions. FT-IR spectra were collected using a spectrometer (Thermo 200). The spectral resolution was 2 cm^{-1} and the spectra were measured from 400 to 4000 cm^{-1}, while the analyzed spectra were from 400 to 1600 cm^{-1}, in absorbance mode. At room temperature, the optical absorbance was recorded using a spectrophotometer (JASCO-V-670) in the 190–2500 nm wavelength span. Finally, Mössbauer spectroscopy was measured using ^{57}Fe transmission Mössbauer spectrometer at room temperature. ^{57}Co (RH) is utilized as a source of γ-radiation. Besides, (α-Fe) is a metallic powder absorber that was exploited for calibrating of velocity and isomer shift of Mössbauer spectra. The current spectra were standardly normalized to relinquish variations in all samples. Gaussian functions software was utilized to decompose the broadened spectra.

3. Results and discussion

3.1. XRD patterns

Fig. 1 presents X-ray diffraction (XRD) patterns for selected glass samples (0 Si and 40 Si). The spectra exhibit no traces of crystalline phases (i.e., no continuous or discrete sharp peaks). The absence of well-defined diffraction peaks rules out the occurrence of the long-range atomic arrangement and, therefore, clearly confirms the amorphous structure of the samples.

3.2. Density measurement

Density is a reliable technique for measuring the glass network's macrostructural and geometrical changes. Fig. 2 illustrates the impact of SiO_2 content on the propensity of density and molar volume of all

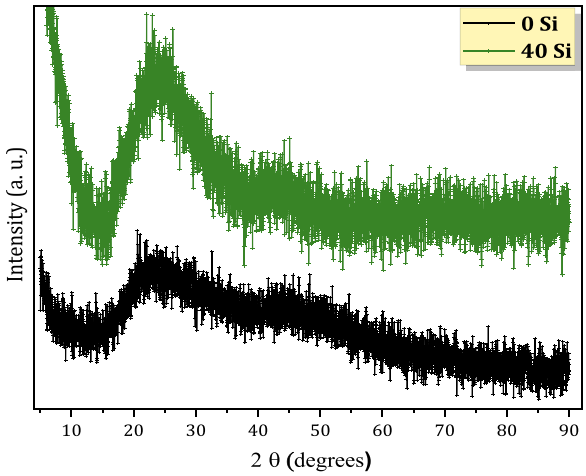

Fig. 1. XRD patterns for selected glass samples (0 Si and 40 Si).

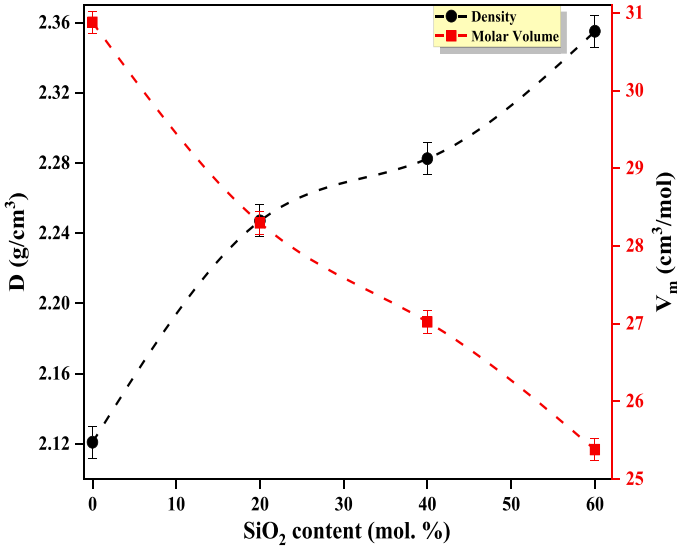

Fig. 2. The density, *D,* and molar volume, V_m against SiO_2 content additives.

samples. Fig. 2 displays that the density of current glass samples increased with the progressive addition of SiO_2 concentration in samples. The obtained density of the glasses can be explained by changing the glass network former. The density of silicon oxide (2.65 g/cm^3) is larger than the density of boron oxide (2.46 g/cm^3). An important factor responsible for the increase in density is the induced changes in the boron-to-oxygen ratio. The progressive addition of SiO_2 content leads to converting the BO_3 units to BO_4 units, combined with the creation of SiO_4 units, which increases the connectivity and compactness of glass samples (i.e., the atoms in the glass network are more tightly packed to each other) [8]. Furthermore, the coordination number is an important factor in following the density behavior; the coordination number of silicon oxide (SiO_4) is greater than that of boron oxide (BO_3). The bond density should be calculated to confirm the coordination number changes according to the following equation [18,19]:

$$n_b = \left(\frac{N_A}{V_m}\sum_i n_f\right), n_f = n_c x_i \quad (1)$$

where n_c is the coordination number of cations B^{3+} (3), Si^{4+} (4), Li^{+} (4), and Fe^{3+} (6) cations. In addition, N_A is Avogadro's number and V_m is the molar volume. The attained values of the bond density are presented in Table 2. The increase in the bond density (i.e., the number of bonds per unit volume) is due to the increase in the coordination number with the SiO_2 addition, leading to an increase in the densification of the network. On the other hand, from Fig. 2, the values of molar volume (V_m) were found to mitigate with the SiO_2 addition. Such changes in molar volume can be explained through average Si-Si distance variations, as discussed later.

The Si^{4+} ions concentration (N_{Si}) was calculated from the following equation [19,20]:

$$N_{Si} = \left[\frac{N_A * mole\ \ fraction\ \ of\ \ SiO_2}{V_m}\right] \quad (2)$$

The obtained values of the Si^{4+} ions concentration were recorded in Table 2. It was observed that the values of N_{Si} increased due to the doping process, this monotonic enhancement causes the network to become more crowded with Si^{4+} ions, increasing the compactness and enhancing the density of the network. The values of Si^{4+} ions concentration was normalized with respect to SiO_2 molar content. The molar concentration is fixed to $\sim (22.28 \pm 0.013) \times 10^{21}$ (cm^{-3}. mol. %) which is the concentration of silicon ions introduced by every 1 mol% of SiO_2 additives. Such a constant value assures the right stoichiometry of the prepared glasses, with negligible loses in the intended SiO_2 doping level during the whole preparation process.

The average Si-Si distance (R_{Si-Si}) was calculated according to the following equation [20,21]:

$$R_{Si-Si} = \left[\frac{1}{N_{Si}}\right]^{1/3} \quad (3)$$

where N_{Si} is Si^{4+} ions concentration. The obtained values of the average Si-Si distance are recorded in Table 2. The diminution in average Si-Si distance from 0.617 nm reaching 0.413 nm with the addition of SiO_2 content is due to the drastic modification in the network. The substitution of B_2O_3 with SiO_2 reduced the bond length in the network, confirming the decrease in the molar volume. We can conclude that the experimental density increased while the calculated molar volume decreased with the progressive addition of SiO_2 content, reflecting more

Table 2
Density (ρ), bond density (n_b), molar volu$_m$e (V_m), Si^{4+} ions concentration (N_{Si}), Si^{4+} ions molar concentration (N_m), and average Si-Si distance (RSi-Si) of all glass samples.

Sample (mol%)	ρ (g/cm^3) ± 0.043	n_b (×10^{19} m^{-3})	V_m (cm^3/mol) ± 0.554	$N_{Si^{4+}}$ (×10^{21}/cm^3) ± 0.274 × 10^{21}	R_i(nm) ± 0.0037	N_m (×10^{22}) (cm^3.mol. %)$^{-1}$ ± 0.0013 * 10^{22}
0 Si	2.121		30.878	0	0	0
		6.35				
20 Si	2.247		28.296	4.256	0.617	2.128
		7.19				
40 Si	2.282		27.021	8.914	0.482	2.228
		8.16				
60 Si	2.355		25.378	14.237	0.413	2.372
		8.89				

network densification, with a propensity to close structures.

3.3. Fourier transform infrared spectroscopy

FTIR is a popular technique in identifying the molecular structure of materials. The modifications in the characteristic mode of the infrared absorption bands reflect the occurring alteration in the chemical and molecular composition of the samples. In this article, the FT-IR was exploited to induce the alteration resulting from the insertion of silicon oxide. Fig. 3 displays the Fourier transform infrared spectra for the four samples. The figure shows a set of characteristic bands located from 400 cm^{-1} to 1550 cm^{-1}. The glass samples are made up of two glass former oxides (namely, B_2O_3 and SiO_2). Therefore, it is plausible that the FT-IR spectra consist of the structural groups of borate and silicate glasses, and the glass is known as borosilicate glasses. As a result, the obtained infrared spectra are like that studied in the literature [6,7,22]. A brief assignment of the resulting peaks was tabulated in Table 3. The first band of spectra consists of a set of characteristic absorption bands of metal ions, such as that located at 434 cm^{-1} that is primarily attributed to lithium ions [7,8]. While the located band at 474 cm^{-1} is attributed to the vibrations of FeO_6 unit [14,16,17]. The bending vibration of B-O-B bonds is pinned at 546 cm^{-1}, when borate rings are deformed [23,24]. The characteristic vibratios of BO_3 are located at in spectral span of (610–750 cm^{-1}). Specifically, these bands were decomposed, using the Gaussian deconvolution process, into three peaks at 669, 700, 780 cm^{-1}. The asymmetric bending vibrational band of O-B-O in bridge oxygen in BO_3 groups was pinned at 669 cm^{-1} [8,23,24]. While the symmetric bending vibrational bands of O-B-O in bridge oxygen in BO_3 groups were pinned at 700 and 780 cm^{-1} [25,26]. Moreover, the stretching vibrations of four-coordinated boron atoms were observed in a spectral span of (751–1190) cm^{-1} [13,14,17]. These stretching bands are allocated to the B-O stretching rocking motions of BO_4 units. Tunning back to trigonal boron (BO_3) units, they have characteristic peaks that are pinned in the spectral domain (1191–1550 cm^{-1}) [13,17,23,27]. This spectral band was deconvoluted to three peaks at 1228, 1369, 1456 cm^{-1}. These peaks are assigned to B-O asymmetric stretching vibrations of BO_3 units. While the first peak among them, which is enveloped at 1228 cm^{-1}, is related to B-O symmetric stretching vibrations of non-bridging oxygens $(NBOs)_{BO_3}$ [8,23,28].

As SiO_2 was inserted into the glass composition, harsh modifications were observed in the intensity and position. Tracing these modulations gives extra information about the glass structure. The enhancement in the absorption spectra through the spectral region (400–600 cm^{-1}) is related to Si-O-Si bonds [2,6,7], and the harsh intensity increment in such spectral region is due to the Si-O-Si [2]. The asymmetric stretching vibrational bands of Si-O-Si bonds created an absorption band at 965 cm^{-1} [2,22]. Moreover, the silicon bonds associated with boron bonds exhibit a broad absorption band (B-O-Si) around 1063 cm^{-1} [6]. Astonishingly, in the spectral range of (751–1190 cm^{-1}), the addition of silicon oxide (i.e., the creation of Si-O-Si and B-O-Si bonds) is mainly responsible for the drastic intensity increment and the shift in position toward the high wavenumber (high energy). In contrary, the addition of silicon oxide has a reverse impact on the intensity and position of the spectral band in the range of (1191–1550 cm^{-1}). A harsh mitigation in the intensity was observed besides a wide shift in the position toward the high energy. For example, by looking into the band at 1228 cm^{-1}, one can observe that with the silicon addition, the intensity harshly reduced (gray highlighted), and the area under peaks deteriorated from 0.9438, 0,4525, 0,3586 to 0.2863, while the position of this band was shifted from 1234, 1253, 1280 and 1365 cm^{-1} (black arrow). Such changes imply the deterioration in NBO bonds in the structure. Generally, along the spectra, it is noted that the intensity of BO_3 units in their two spectral regions was drastically mitigated, in contrast to the intensity of BO_4

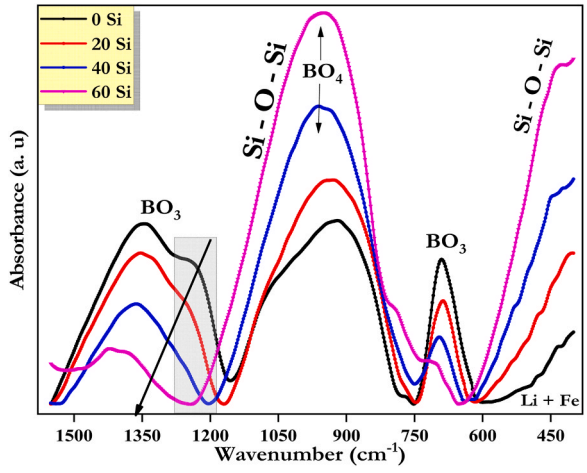

Fig. 3. FT-IR spectra of all samples, showing the important structural units, and the highlighted part shows the NBO mitigation with SiO_2 content additives.

Table 3
FTIR peak positions together with brief assignments of all borosilicate glass samples.

Refs.	Wavenumber (cm^{-1}) Assignments				
	0 Si	20 Si	40 Si	60 Si	
[7,8]	435	433	435	434	Lithium ionic vibrations.
[14, 16, 17]	477	473	473	473	Iron ionic vibrations.
[2,6, 7]	——	512	511	511	Si-O-Si bonds
[22, 23]	515	556	556	558	B-O-B bending vibrations of angle's deformations.
[8, 22, 23]	651	664	675	685	Asymmetric O-B-O bending vibrations of bridge oxygen in BO_3 groups.
[24, 25]	691	694	700	715	Symmetric O-B-O bending vibrations of bridge oxygen in BO_3 groups.
[24, 25]	777	780	782	780	
[13, 14, 17]	854–1048	832–895	838–901	840–902	B-O stretching vibrations and rocking motion of tetrahedral BO_4units.
[2, 13, 17, 21]	974	979	978	974	B-O stretching vibrations and rocking motion of tetrahedral BO_4units/asymmetric stretching vibrations of Si-O-Si bonds
[6]	1059	1067	1068	1059	B-O stretching vibrations and rocking motion of tetrahedral BO_4units/stretching vibrations of B-O-Si
[8, 22, 26]	1234	1253	1280	1365	B-O symmetric stretching vibrations of non-bridging oxygens of trigonal units, $(NBOs)_{BO_3}$.
[13, 17, 22]	1337	1348	1363	1430	B-O asymmetric stretching vibrations of BO_3 units
[13, 19, 22]	1404	1455	1446	1520	

units that was observed to enhance. Such changes proved the embedding of silicon oxide into a glass host leads to transform of BO_3 units into BO_4 units, together with mitigation of the number of NBO through creating Si-O-Si and B-O-Si bonds.

3.4. Optical properties

3.4.1. Ligand field parameters

The non-destructive optical properties of [SiO_2-B_2O_3-Li_2O-Fe_2O_3] glass system were investigated. Fig. 4 displays the normalized absorption spectra of the synthesized glass samples at RT. The detector sensitivity at 360 nm was accurately treated. It is monitored that the spectra have a set of characteristic absorption bands related to the existence of Fe ions in the samples. Besides the absorption edges and Urbach tails at high-energy region. The absorption bands related to the existence of Fe ions were found to undergo a spectral overlapping for all the samples. When the B_2O_3 was substituted by SiO_2, the optical absorption bands become more clear and undergo small shifts. So, a decomposition process should be executed to the overlapped absorption spectra to relinquish the overlapping in such bands and obtain more information about these bands. As a representative example, the deconvolution process is now presented in Fig. 5, for sample 20 Si. The outcome Gaussian deconvoluted bands were seven at wavelengths ~ 402.13 nm (labeled as ν_7), ~ 452.52 nm (labeled as ν_6), ~ 513.25 nm (labeled as ν_5), ~ 602.25 nm (labeled as ν_4), ~ 701.25 nm (labeled as ν_3), ~ 795.5 nm (labeled as ν_2) and ~ 948 nm (labeled as ν_1), Fig. 5.

To go into further detail concerning such bands, the bands ν_7, ν_6, ν_5, ν_4, and ν_3 are related to the optical electronic transitions of Fe^{3+} cations due to the interaction with the ligand field in tetrahedral (T_d) symmetry. Such bands represent the transitions from the ground state of tetrahedral Fe^{3+} ions [$^6A_1(^6S)$] to the excited states [$^4E(^4D)$, $^4T_2(^4D)$, $^4T_2$, $^4E(^4D)$, $^4T_2(^4G)$, and $^4T_1(^4G)$], respectively [17,29–31]. While the bands ν_2 and ν_1 are related to the transitions of Fe^{3+} ions in octahedral (O_h) symmetry and assigned to the transitions from the ground state of octahedral Fe^{3+} ions [$^6A_{1g}(^6S)$] to the excited states [$^4T_{2g}(^4G)$ and $^4T_{1g}(^4G)$], respectively [13,17,30,32].

The ligand field splitting (*10 Dq*) and Racah parameters (*B* and *C*) were calculated using the expressions developed by Tanabe-Sugano for energy states in ***tetrahedral symmetry*** (T_d) of Fe^{3+} cations [17,33,34]. Based on the deconvoluted transitions ν_7 and ν_6, the energy equations are given as [34,35]:

$$^6A_1(^6S)\rightarrow{}^4E\quad(^4D)\quad = 17B + 5\quad C \sim\quad \nu_7 \tag{4}$$

$$^6A_1(^6S)\rightarrow{}^4T_2\quad(^4D)\quad = 13B + 5\quad C \sim\quad \nu_6 \tag{5}$$

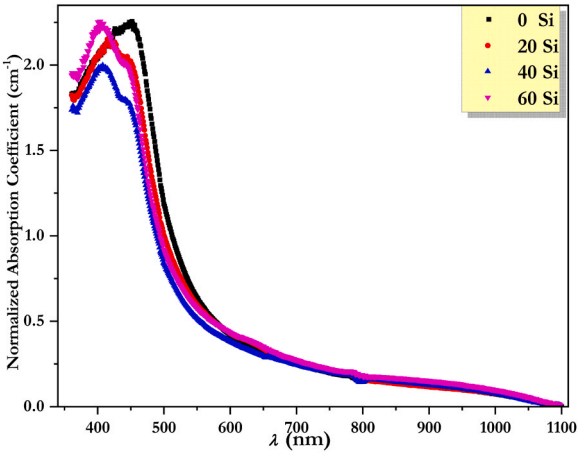

Fig. 4. Optical absorption Spectra against the wavelength for all prepared samples.

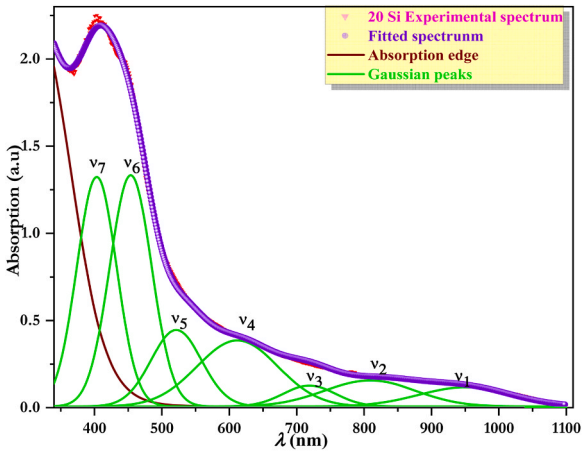

Fig. 5. Gaussian deconvolution process showing the isolated Fe-related bands with their nominal assign, for sample (20 mol%) as a representative example.

These energy equations were exploited to deduce Racah parameters (*B* and *C*) as follows:

$$B = (\nu_7 \quad - \quad \nu_6)/4 \tag{6}$$

$$C = (17\nu_6 - 13\nu_7)/20 \tag{7}$$

while the energy equation of the band ν_4 was given as follows:

$$^6A_1(^6S)\rightarrow{}^4T_2\quad(^4G) = -10Dq + 18B + 6\quad C - \quad 38B^2/10Dq \sim\quad \nu_4 \tag{8}$$

This important energy equation is exploited to extract the ligand field strength (10 Dq):

$$^6A_1(^6S)\rightarrow{}^4T_2\quad(^4G) = -10Dq + 18B + 6\quad C - 38B^2/10Dq \sim \nu_4 \tag{9}$$

The obtained values of 10 Dq, (B and C), and Dq/B are listed in Table 4. The 10 Dq values increased with the addition of SiO_2 content. While Racah parameters (B and C) were found to decrease as SiO_2 content increased, as shown in Fig. 6. The increase in 10 Dq values is attributed to the increase in the oxygen concentration in the composition due to the substitution of B_2O_3 content with the structural unit (BO_3) by SiO_2 content with the structural unit (SiO_4). This substitution leads to enhance the environment of anions around Fe^{3+} ions, and in its turn, leads to augment the interaction between the 3d orbitals of Fe^{3+} ions and the surrounding ligands, increasing the splitting energy of orbitals. As well as, the higher energy levels of Si than that of B are an influential factor in increasing 10 Dq values. Where the internal electronic configuration of the Si atom is $1S^2$, $2S^2$, $2P^6$, $3S^2$, $3P^6$ compared to that of B atom $1S^2$, $2S^2$, $2P^1$. The 3 P orbital is more diffused and lesser bonded with the nucleus of Si than the 2 P orbital, which is highly tightened with the nucleus of the B atom. So, the 3 P orbital of the Si ion is high interact with the orbital of Fe^{3+} ions. As a result, the increasing splitting between 3d orbitals of Fe^{3+} ions, enhancing the 10Dq values.

On the other hand, the increase in the splitting of 3d orbitals leads to mitigating the interelectronic repulsion between electrons inside the *d*-level of Fe^{3+} ions, decreasing Racah parameters (B and C).

Ligand field theory provides additional information about the bonding nature between the Fe^{3+} ions and their surrounding field. The nephelauxetic ratio (β) is the oldest parameter to rationalize the interelectronic energy. It is determined from the ratio between Racah B parameter for our glasses and iron-free ion [35]: [$\beta = B/B_o$], where B_o of iron free ion is 1015 cm^{-1}. The nephelauxetic ratio values were recorded in Table 4. The decreasing trend of such values implies that there is a decreasing in ionicity of bond nature between Fe^{3+} ions and their surrounding filed [8]. For more going in the bond nature confirmation, a new modification was proposed by Brik and Srivastava [36,37], by

Table 4
Ligand field strength (10 *Dq*), Racah parameters (*B* and *C*), nephelauxetic ratio (β), nephelauxetic parameter (β_1), nephelauxetic effect (*h*), average reduction factor (N^2), *Dq/B* ratio, and *C/B* ratio of all glass samples.

Sample (mol%)	10 Dq (cm^{-1})	B (cm^{-1})	C (cm^{-1})	β	β_1	h	N^2	Dq/B	C/B
0 Si	9388	695	2630	0.684	0.877	1.313	0.783	1.35	3.784
20 Si	9687	694	2625	0.683	0.875	1.317	0.783	1.39	3.782
40 Si	9753	690	2614	0.679	0.871	1.332	0.781	1.41	3.788
60 Si	9942	689	2611	0.678	0.869	1.337	0.780	1.44	3.789

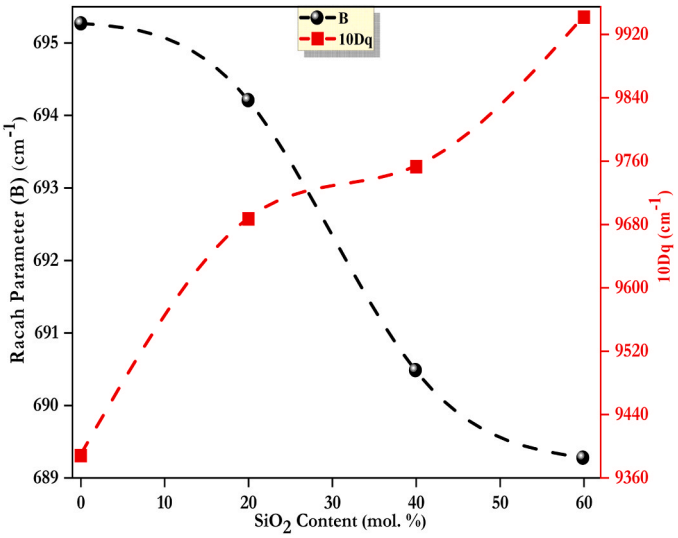

Fig. 6. The splitting magnitude (*10 Dq*) and Racah parameter (*B*) against SiO_2 content additives.

insertion of the Racah C parameter for accurate determining of the nephelauxetic effect. The novel parameter is called the nephelauxetic parameter (β_1), which is calculated from the following relation [36,37]:

$$\beta_1 = \sqrt{(\frac{B}{B_o})^2 + (\frac{C}{C_o})^2} \quad (10)$$

Brik and Srivastava [36,37] proposed a successful attempt to treat the defect in nephelauxetic ratio ($\beta = B/B_o$). The nephelauxetic ratio ($\beta = B/B_o$) describes the electronic cloud in d-orbitals only relied on Racah B parameters. However, both Racah (B and C) parameters were embedded in nephelauxetic calculations for the novel parameter. The attained values of the β_1 are reported in Table 4. The decrease in β_1 values with the addition of SiO_2 content is due to the high delocalization of electrons in d-orbitals, that in its turn support the electron transfer between ions to create covalent bonds, rendering the bonding nature between Fe^{3+} cations and their ligands are more covalent.

For a more detailed discussion of the spectroscopic behavior, the nephelauxetic effect (*h*) is exploited in discussing the bonding nature properties. The nephelauxetic effect (*h*) is determined from the expression:

$$h = \frac{[(B_o - B)/B_o]}{k_{Fe^{3+}}} \quad (11)$$

where *k* is a parameter that characterizes the transition metal ion, and B_o is the Racah parameter for free Fe^{3+} cation. $k = 0.24$ and $B_o = 1015$ cm^{-1} [1,9,12]. Larger values of *h* (see Table 4) imply a decrease in the localization of *d*-electrons of Fe^{3+} ions and increasing the covalent nature of Fe^{3+}- ligand bonding [17].

Furthermore, the covalency reduction factor, N^2, describes the covalency of bonding nature in materials. The covalency reduction factor can be computed from the following relationship [24,38,39]:

$$N^2 = \frac{1}{2}(\sqrt{\frac{B}{B_o}} + \sqrt{\frac{C}{C_o}}) \quad (12)$$

when the covalency reduction factor increases, the covalency of bonding nature deteriorates and vice-versa. The N^2 values are registered in Table 4. The decrease in covalency reduction factor relates to the increment in covalency effects with the addition of SiO_2 content (i.e., minimization of the interelectronic repulsion force of 3d-electrons of Fe^{3+} ions).

3.4.2. Band gap energy

Studying the impact of composition modification on the high energy region (i.e., Tauc region) in the absorption spectra is an interesting subject to extract the optical parameters. The impact of SiO_2 addition on Tauc's region (i.e., the absorption edges) caused marginal variations, reflecting small changes in extracted optical parameters. The optical absorption coefficient were obtained from the following relation:

$$\alpha(\nu) = 2{\cdot}303(A/d) \quad (13)$$

where $\alpha(\nu)$ is optical absorption coefficient, *A* is the optical absorbance, and *d* is thickness of samples. The optical absorption spectra of all samples were presented in Fig. 4. Mott and Davis [40] exploited the optical absorption coefficient to evaluate the optical band gap E_{opt} of the synthesized glass using the following equation:

$$\alpha h\upsilon = q(h\upsilon - E_{opt})^m \quad (14)$$

where $h\nu$ is the incident photon energy, and *q* is the band tailing parameter. The index *m* is taken the values 1/2, 2, 2/3, or 3. The best choice is based on the type of electronic transition: (direct allowed, indirect allowed, direct forbidden, and indirect forbidden) transition, respectively. The indirect allowed transition is the possible transition in the glass materials [8]. The E_{opt} was evaluated via drawing a graph between $(\alpha h\nu)^{0.5}$ (as Y-axis) and $h\nu$ (as X-axis), (i.e., Tauc's plot), then by determining the intersect position of the first linear part with $h\nu$ axis at $[(\alpha h\nu)^{0.5} = 0]$ [24]. The obtained E_{opt} values were listed in Table 5. The E_{opt} values were found to marginally mitigate from 2.668 eV to 2.626 eV, as SiO_2 content increased. Such scant decrease in E_{opt} values is due to the mixed former effect that here increases the oxygen concentration in the composition, as well as the higher energy levels of Si atom than that of B atom contributes to decrease the E_{opt} values, as discussed

Table 5
Optical band gap energy (E_g), metallization criterion (*M*), linear refractive index, third order non-linear optical susceptibility, and non-linear refractive index of all glass samples.

Sample code (mol %)	E_g (eV)	$M(eV)^{0.5}$	n_0	$\chi^{(3)}$ ($\times 10^{-14}$)(esu)	n_2 ($\times 10^{-13}$)
0 Si	2.668	0.365	1.456	1.069	2.771
20 Si	2.654	0.364	1.471	1.243	3.189
40 Si	2.638	0.363	1.475	1.296	3.315
60 Si	2.626	0.362	1.483	1.410	3.585

before. The scant decrease in the values of E_{opt} is compatible with the decrease in the localization of d-electrons of Fe^{3+} ions and the increase in the covalency of Fe^{3+} ions - ligand bonding. In more details, the delocalization of electrons of ions and covalency are closely related concepts. Covalency is a measure of the sharing of electrons between ions, and the delocalization of electrons is a form of covalent bonding. In other words, when the electrons of an ion are delocalized, they are shared with the other ion in the molecule or crystal. Therefore, the delocalization of electrons is associated with covalent interactions through the transfer of electrons between ions. This transfer of electrons creates a covalent bond between the molecules, which is considered a characteristic of covalent interactions in glass material [41,42].

Furthermore, the metallization criterion (M) is an informative parameter that predicts the material's nature (metals, semiconductors, or insulators). The metallization criterion is obtained using the E_{opt} values from the following relation [23,43]:

$$M = (E_g/20)^{0.5} \tag{15}$$

The value of the metallization criterion was scaled between two sets (0) and (1). The center between them predicts the semiconductor nature. The material behaves as metal when the M value moves to (0). The material behaves as an insulator when the M value nears (1). Here, the attained values of M were reported in Table 5. The M values were found to fix at 0.36 $(eV)^{0.5}$ indicates that with the former-former replacement has a marginal effect on the semiconducting nature of the prepared samples.

3.5. Non-linear properties

The non-linear properties are a paved route towards understanding the quality of optical features of the glass samples. The non-linearity of materials is decided by some of the properties, such as linear refractive index (n_o), non-linear refractive index (n_2), and optical susceptibility (χ). The linear refractive index (n_o) was calculated using a relationship mentioned elsewhere [8]. The obtained values of the linear refractive index are recorded in Table 5. The increase in linear refractive index is due to the density increment and the inter-ionic variations, as the ionic radius of Si^{4+} ion (50 pm) is higher than that of B^{3+} ion 25 pm. The third-order non-linear susceptibility (χ^3) could be appraised from the linear refractive index using the subsequent equation [38,44]:

$$\chi^3 = \frac{A}{256\pi^4}[(n^2-1)^4] \tag{16}$$

where $A = 1.7\times10^{-10}$ esu. The non-linear refractive could be obtained from optical susceptibility using the following relationship [38,44]:

$$n_2 = \frac{12\pi}{n}\chi^3 \tag{17}$$

The values of both χ^3 and n_2 were depicted in Table 5. The values show both of χ^3 and n_2 to enhance with the SiO_2 content addendum, implying that the SiO_2 doping improved the non-linear characteristics of our materials. As highlighted previously, the mitigation in E_{opt} was observed to improve the non-linear properties. This trend renders these glasses more suitable for high-tech applications, including optical waveguides and switching, image processing and manipulation [44,45]. Furthermore, Fig. 7 depicts the linear relationship between the optical susceptibility and the inverse of optical gap energy. It is observed that the highest non-linear susceptibility was attained at the minimum value of the optical band gap. Such linear relation indicates that the enhancement in the non-linear properties of the prepared samples is tunable by E_{opt}.

3.6. Mössbauer spectroscopy

Mössbauer spectra of the current glasses were measured and presented in Fig. 8. A packaged software based on Voigt profiles was used to obtain the hyperfine interaction parameters to analyze and extract the required information. The analyzed spectra exhibited three polymorphic phases of iron cations in the glasses. Fe^{3+} ions with an isomer shift of (0.285–0.314) mm s^{-1} in Td sites, Fe^{2+} ions with an isomer shift at about 0.905 mm s^{-1} in T_d sites and Fe^{3+} ions with an isomer shift of (0.425 – 0.339) mm s^{-1} in O_h sites [17,46,47]. The existence of Fe^{3+}_{Td} and Fe^{3+}_{Oh} phases in Mössbauer spectra are compatible with the optical results. While the absence of the Fe^{2+}_{Td} phase in the optical spectra is due to the weakness of its optical-electronic transition [$^5E(D)\rightarrow{}^5T_2(D)$] that occurs at wavelength of 2222 nm [48]. Mössbauer parameters, including isomer shift (IS), quadrupole splitting (QS), widths of Gaussian distribution (GW), relative area of each phase (Fe^{3+}_{Td}%, Fe^{2+}_{Td}%, and Fe^{3+}_{Oh}%) were listed in Table 6. The decrease in the isomer shift of the three phases, with further addition of SiO_2 content, can be explained by the increase in oxygen concentration in the composition, leading to increase the oxygen concentration around iron ions, this in its turn causes an increase in electron density around iron ions and a subsequent decrease in the isomer shift. This finding is consistent with the obtained results from the ligand field analysis (i.e., the increase in *10 Dq* and *h* parameters). The increase in *10 Dq* indicates a strong effect of the ligand anions on the iron ions, increasing the splitting of *d* orbitals in iron cations. While the nephelauxetic effect, *h*, suggests an increase in the covalency of bonding nature between Fe^{3+}-ligands, confirming a shortened bond length between the ligand anions and iron cations. In addition, the observed

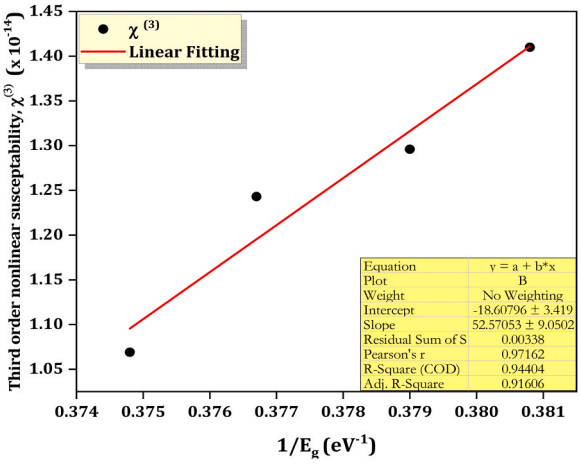

Fig. 7. The third-order non-linear optical susceptibility against the inverse of optical band gap energy.

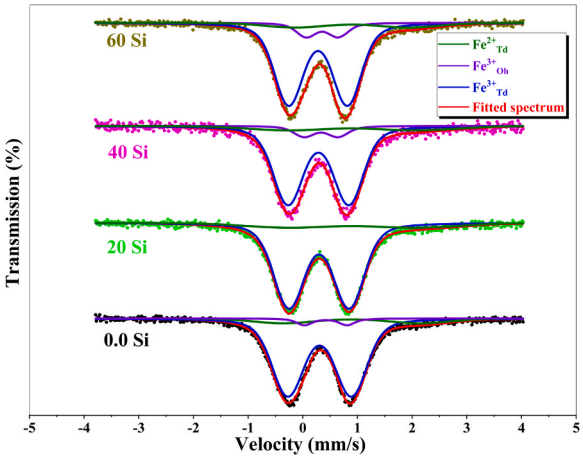

Fig. 8. Mössbauer spectra for all glass samples.

Table 6
Mössbauer parameters including isomer shift (IS), quadrupole splitting (QS), widths of Gaussian distribution (GW), and relative area for each phase (Fe^{3+}_{Td}%, Fe^{2+}_{Td}%, and Fe^{3+}_{Oh}%) of the prepared glass samples.

Sample code	Fe^{3+}_{Td}			Fe^{2+}_{Td}			Fe^{3+}_{Oh}			Fe^{3+}_{Td} %	Fe^{2+}_{Td} %	Fe^{3+}_{Oh} %
	IS (mm s^{-1})	QS (mm s^{-1})	GW (mm s^{-1})	IS (mm s^{-1})	QS (mm s^{-1})	GW (mm s^{-1})	IS (mm s^{-1})	QS (mm s^{-1})	GW (mm s^{-1})			
0 Si	0.314	1.164	0.231	0.906	2.529	0.509	0.425	0.768	0.072	0.861	0.098	0.041
20 Si	0.304	1.103	0.221	0.903	2.369	0.760	—	—	—	0.871	0.129	—
40 Si	0.291	1.113	0.212	0.904	2.364	0.677	0.339	0.620	0.129	0.807	0.110	0.083
60 Si	0.285	1.075	0.203	0.905	2.098	0.505	0.362	0.585	0.120	0.806	0.091	0.103

decrease in quadrable splitting, QS, in all phases of iron ions is attributed to the increase in the symmetry of the surrounding anions around iron ions. Initially, such increased symmetry originates from the decrease in the polarization power of the glass former cations with further addition in SiO_2 content [49]. Polarization power is the ability of a cation (here, Fe) to distort the electronic cloud of an anion [50]. The polarization power of B^{3+} is (247.9 e/Å for tetrahedral coordination sites and 41.2 e/Å for octahedral coordination sites). While the polarization power of Si^{4+} is (59.2 e/Å for tetrahedral coordination sites and 25.0 e/Å for octahedral coordination sites). The polarization power of cations was calculated based on the relation Q/r^2, where Q and r are the cation's ionic charge and ionic radius, respectively [49,51]. The replacement of B_2O_3 by SiO_2 was found to decrease the polarization power of the formers, which leads to an enhancement in the symmetry of the electron cloud of the anions around iron ions and decreases the QS values.

4. Conclusion

In summary, we reported the preparation and investigation of Fe_2O_3 and Li_2O containing borosilicate glass. Fe_2O_3 and Li_2O containing a borosilicate glass system was prepared using the classical melt-quenching method. The structural variations on the macro scale were investigated through mass density and related parameters. The density increased with SiO_2 additions, while the molar volume decreased. The vibrational analysis confirmed a strong conversion to BO_4 and SiO_4 structural units, accompanied by mitigation in NBOs content. This result agrees with density results in that the network became harder and densified. Furthermore, optical electronic transitions (402–948 nm) of Fe ions were assigned and proved the existence of iron ions in the trivalent state with tetrahedral and octahedral coordination. The ligand field parameters of Fe ions in tetrahedral symmetry were calculated by exploiting the energy positions of these electronic transitions. The ligand field splitting increased (9388–9942 cm^{-1}), confirming the augmentation in the interaction between the 3d orbitals of Fe^{3+} ions and the surrounding ligands. While the decrease in Racah parameters, B (695–689 cm^{-1}) and C (2630–2611 cm^{-1}), confirming the decrease in interelectronic repulsion of 3D-electrons, with further SiO_2 additions. The nephelauxetic parameter, nephelauxetic ratio, and covalency reduction factor confirmed that the bonding nature, between Fe ions and their ligands, is more ionic (less covalent). Moreover, the optical band gaps were calculated using Tauc's plots and justified by mixed former effect. Additionally, metallization criterion values were settled down at 0.36 $eV^{0.5}$, confirming the semiconductor nature of samples, whereas non-linear features were increased with further SiO_2 additions. The decrease in optical gap energy justified this propensity. Astonishingly, Mössbauer spectra helped in unveiling polymorphic phases of iron ions. And calculating both isomer shift and quadrable splitting of these phases. The electronegativity concept explained the decrease in isomer shift and agreed with ligand filed splitting behavior. While the polarization power of mixed former cations justified the decrease in quadrable splitting.

Author agreement statement

We the undersigned declare that this manuscript is original, has not been published before and is not currently being considered for publication elsewhere. We confirm that the manuscript has been read and approved by all named authors and that there are no other persons who satisfied the criteria for authorship but are not listed. We further confirm that the order of authors listed in the manuscript has been approved by all of us. We understand that the corresponding author is the sole contact for the Editorial process. He is responsible for communicating with the other authors about progress, submissions of revisions and final approval of proofs.

Declaration of Competing Interest

The authors declare that they have no known competing financial interests or personal relationships that could have appeared to influence the work reported in this paper.

Data Availability

Data will be made available on request.

References

[1] D. Zhang, W. Xiao, C. Liu, X. Liu, J. Ren, B. Xu, J. Qiu, Highly efficient phosphor-glass composites by pressureless sintering, Nat. Commun. 11 (2020) 1–8, https://doi.org/10.1038/s41467-020-16649-z.
[2] Z.M. Abd El-Fattah, F. Ahmad, M.A. Hassan, Tuning the structural and optical properties in cobalt oxide-doped borosilicate glasses, J. Alloys Compd. 728 (2017) 773–779, https://doi.org/10.1016/j.jallcom.2017.09.059.
[3] M.A. Karakassides, A. Saranti, I. Koutselas, Preparation and structural study of binary phosphate glasses with high calcium and/or magnesium content, J. Non Cryst. Solids 347 (2004) 69–79, https://doi.org/10.1016/j.jnoncrysol.2004.08.111.
[4] J. Anjaiah, C. Laxmikanth, N. Veeraiah, Spectroscopic properties and luminescence behaviour of europium doped lithium borate glasses, Phys. B Condens. Matter 454 (2014) 148–156, https://doi.org/10.1016/j.physb.2014.07.070.
[5] Y.S.M. Alajerami, S. Hashim, S.K. Ghoshal, M.A. Saleh, T. Kadni, M.I. Saripan, K. Alzimami, Z. Ibrahim, D.A. Bradley, The effect of TiO2 and MgO on the thermoluminescence properties of a lithium potassium borate glass system, J. Phys. Chem. Solids 74 (2013) 1816–1822, https://doi.org/10.1016/j.jpcs.2013.07.013.
[6] M. Farouk, D.A. Slibi, Z.M. Abd El-Fattah, M. Atallah, M.A. El-Sherbiny, M. A. Hassan, Effect of SiO2 addition on chromium transitions in borate glasses, Silicon 13 (2021) 3003–3010, https://doi.org/10.1007/s12633-020-00649-1.
[7] M.G. Moustafa, H. Morshidy, A.R. Mohamed, M.M. El-Okr, A comprehensive identification of optical transitions of cobalt ions in lithium borosilicate glasses, J. Non Cryst. Solids 517 (2019) 9–16, https://doi.org/10.1016/j.jnoncrysol.2019.04.037.
[8] H.Y. Morshidy, A.R. Mohamed, A.A. Abul-magd, M.A. Hassan, Ascendancy of Cr 3 + on Cr 6 + valence state and its effect on borate glass environment through CdO doping, Mater. Chem. Phys. 285 (2022), 126128, https://doi.org/10.1016/j.matchemphys.2022.126128.
[9] A. Bhogi, P. Kistaiah, Alkaline earth lithium borate glasses doped with Fe (III) ions -an EPR and optical absorption study, Mater. Today Proc. 5 (2018) 26199–26206, https://doi.org/10.1016/j.matpr.2018.08.068.
[10] T. Sugawara, R. Komatsu, S. Uda, Linear and nonlinear optical properties of lithium tetraborate, Solid State Commun. 107 (1998) 233–237, https://doi.org/10.1016/S0038-1098(98)00190-2.
[11] P. Kluvánek, R. Klement, M. Karáčoň, Investigation of the conductivity of the lithium borosilicate glass system, J. Non Cryst. Solids 353 (2007) 2004–2007, https://doi.org/10.1016/j.jnoncrysol.2007.01.064.

[12] C.E. Kim, H.C. Hwang, M.Y. Yoon, B.H. Choi, H.J. Hwang, Fabrication of a high lithium ion conducting lithium borosilicate glass, J. Non Cryst. Solids 357 (2011) 2863–2867, https://doi.org/10.1016/j.jnoncrysol.2011.03.022.
[13] A.A. Abul-Magd, A.S. Abu-Khadra, A.M. Taha, A.A.H. Basry, Influence of La3+ ions on the structural, optical and dielectric properties and ligand field parameters of Fe3+ hybrid borate glasses, J. Non Cryst. Solids 599 (2023), 121981, https://doi.org/10.1016/j.jnoncrysol.2022.121981.
[14] A.S. Abu-khadra, M.S. Sadeq, Influence of Fe cations on the structural and optical properties of alkali- alkaline borate glasses, J. Non Cryst. Solids 548 (2020), 120320, https://doi.org/10.1016/j.jnoncrysol.2020.120320.
[15] T. Minami, Fast ion conducting glasses, J. Non Cryst. Solids 73 (1985) 273–284, https://doi.org/10.1016/0022-3093(85)90353-9.
[16] M.S. Sadeq, M.A. Abdo, Effect of iron oxide on the structural and optical properties of alumino-borate glasses, Ceram. Int. 47 (2021) 2043–2049, https://doi.org/10.1016/j.ceramint.2020.09.036.
[17] E.A. Elkelany, M.A. Hassan, A. Samir, A.M. Abdel-Ghany, H.H. El-Bahnasawy, M. Farouk, Optical and Mössbauer spectroscopy of lithium tetraborate glass doped with iron oxide, Opt. Mater. (Amst.) 112 (2021), 110744, https://doi.org/10.1016/j.optmat.2020.110744.
[18] M. Abdel-Baki, F.A. Abdel-Wahab, F. El-Diasty, One-photon band gap engineering of borate glass doped with ZnO for photonics applications, J. Appl. Phys. 111 (2012), https://doi.org/10.1063/1.3698623.
[19] M. Ezzeldin, L.M. Al-harbi, M.S. Sadeq, A.E. Mahmoud, M.A. Muhammad, H. A. Ahmed, Impact of CdO on optical, structural, elastic, and radiation shielding parameters of CdO – PbO – ZnO – B 2 O 3 – SiO 2 glasses, Ceram. Int. (2023), https://doi.org/10.1016/j.ceramint.2023.03.042.
[20] M.I. Sayyed, M.A. Abdo, H.E. Ali, H.A. Ahmed, M.S. Sadeq, Impact of lead oxide on the structure, optical, and radiation shielding properties of potassium borate glass doped with samarium ions, Opt. (Stuttg.) 278 (2023), 170738, https://doi.org/10.1016/j.ijleo.2023.170738.
[21] M.S. Sadeq, M.I. Sayyed, M.A. Abdo, H.E. Ali, A.E. razek Mahmoud, H.A. Ahmed, Compositional dependence of transparency, linear and non-linear optical parameters, and radiation shielding properties in lanthanum, iron and calcium borate glasses, Radiat. Phys. Chem. 212 (2023), 111027, https://doi.org/10.1016/j.radphyschem.2023.111027.
[22] S.F. Mansour, S. Wageh, M.F. Alotaibi, M.A. Abdo, M.S. Sadeq, Impact of bismuth oxide on the structure, optical features and ligand field parameters of borosilicate glasses doped with nickel oxide, Ceram. Int. 47 (2021) 21443–21449, https://doi.org/10.1016/j.ceramint.2021.04.154.
[23] M.M. EL-Hady, H.Y. Morshidy, M.A. Hassan, Judd-Ofelt analysis, optical and structural features of borate glass doped with erbium oxide, J. Lumin. 263 (2023), 119972, https://doi.org/10.1016/j.jlumin.2023.119972.
[24] H.Y. Morshidy, Z.M. Abd El-Fattah, A.A. Abul-Magd, M.A. Hassan, A.R. Mohamed, Reevaluation of C r 6 + optical transitions through G d 2 O 3 doping of chromium-borate glasses, Opt. Mater. (Amst.) 113 (2021), 110881, https://doi.org/10.1016/j.optmat.2021.110881.
[25] E.I. Kamitsos, A.P. Patsis, M.A. Karakassides, G.D. Chryssikos, Infrared reflectance spectra of lithium borate glasses, J. Non Cryst. Solids 126 (1990) 52–67, https://doi.org/10.1016/0022-3093(90)91023-K.
[26] T.R. Rao, C.V. Reddy, C.R. Krishna, U.S.U. Thampy, R.R. Raju, P.S. Rao, R.V.S.S. N. Ravikumar, Correlation between physical and structural properties of Co2+ doped mixed alkali zinc borate glasses, J. Non Cryst. Solids 357 (2011) 3373–3380, https://doi.org/10.1016/j.jnoncrysol.2011.06.004.
[27] H.Y. Morshidy, M.S. Sadeq, A.R. Mohamed, M.M. EL-Okr, The role of CuCl2 in tuning the physical, structural and optical properties of some Al2O3–B2O3 glasses, J. Non Cryst. Solids 528 (2020) 28–29, https://doi.org/10.1016/j.jnoncrysol.2019.119749.
[28] H.Y. Morshidy, A.R. Mohamed, A.A. Abul-Magd, M.A. Hassan, Role of high energy Cr6+ optical transition induced by rare earth ion (La3+) in compositional-dependent borate glass, Mater. Chem. Phys. 289 (2022), https://doi.org/10.1016/j.matchemphys.2022.126503.
[29] L. Alyabyeva, V. Burkov, B. Mill, Optical spectroscopy of La3Ga5SiO4 disordered crystals doped with Fe3+ ions, Opt. Mater. (Amst.) 43 (2015) 55–58, https://doi.org/10.1016/j.optmat.2015.02.023.
[30] V. Vercamer, G. Lelong, H. Hijiya, Y. Kondo, L. Galoisy, G. Calas, Diluted Fe3+ in silicate glasses: Structural effects of Fe-redox state and matrix composition. An optical absorption and X-band / Q-band EPR study, J. Non Cryst. Solids 428 (2015) 138–145, https://doi.org/10.1016/j.jnoncrysol.2015.08.010.
[31] Y. Wang, R.K. Li, d–d Transitions of Fe3+ ions in Fe-doped K2Al2B2O7 crystal 32 (2010) 1313–1316, https://doi.org/10.1016/j.optmat.2010.04.036.
[32] B. Hannoyer, M. Lenglet, J. Dürr, R. Cortes, Spectroscopic evidence of octahedral iron (III) in soda-lime silicate glasses, J. Non Cryst. Solids 151 (1992) 209–216, https://doi.org/10.1016/0022-3093(92)90031-E.
[33] D.M. Sherman, T.D. Waite, Electronic spectra of Fe3+ oxides and oxide hydroxides in the near IR to near UV, Am. Mineral. 70 (1985) 1262–1269.
[34] A.B.P. Lever, 9- Lever -inorganic electronic spectroscopy.pdf, (1984).
[35] S. Sugano, Y. Tanabe, H. Kamimura, Multiplets of transition-metal ions in crystals, Pure Appl. Phys. v. 33 (33) (1970) 331 (xi).
[36] C.G. Ma, Y. Wang, D.X. Liu, Z. Li, X.K. Hu, Y. Tian, M.G. Brik, A.M. Srivastava, Origin of the β1 parameter describing the nephelauxetic effect in transition metal ions with spin-forbidden emissions, J. Lumin. 197 (2018) 142–146, https://doi.org/10.1016/j.jlumin.2018.01.036.
[37] M.G. Brik, S.J. Camardello, A.M. Srivastava, N.M. Avram, A. Suchocki, Spin-forbidden transitions in the spectra of transition metal ions and nephelauxetic effect, ECS J. Solid State Sci. Technol. 5 (2016) R3067–R3077, https://doi.org/10.1149/2.0091601jss.
[38] A.M. Babeer, A.E. Mahmoud, H.Y. Morshidy, Ligand field parameters, optical, thermal, magnetic, and structural features of ZnO containing cobalt-borate glasses, Mater. Chem. Phys. (2023), 143747, https://doi.org/10.1016/j.matchemphys.2023.127681.
[39] S.A. Hussien, E.M. Saad, E.A. Gaber, A.E. razek Mahmoud, H.Y. Morshidy, Impactive cadmium modifications to enhance the structural-optical relationship in nickel borate glasses, Ceram. Int. (2023), https://doi.org/10.1016/j.ceramint.2023.04.124.
[40] P. Taylor, E.A. Davis, N.F. Mott, Conduction in non-crystalline systems V, Conduct. Opt. Absorpt. Photocond. Amorph. Semicond. (2006) 37–41.
[41] X. Wang, X. Fan, X. Yu, S. Bak, Z. Shadike, I. Waluyo, A. Hunt, S.D. Senanayake, H. Li, L. Chen, C. Wang, R. Xiao, E. Hu, X.Q. Yang, The role of electron localization in covalency and electrochemical properties of lithium-ion battery cathode materials, Adv. Funct. Mater. 31 (2021), https://doi.org/10.1002/adfm.202001633.
[42] R. Zimmermann, P. Steiner, R. Claessen, F. Reinert, S. Hüfner, P. Blaha, P. Dufek, Electronic structure of 3d-transition-metal oxides: on-site Coulomb repulsion versus covalency, J. Phys. Condens. Matter 11 (1999) 1657–1682, https://doi.org/10.1088/0953-8984/11/7/002.
[43] V. Dimitrov, T. Komatsu, Electronic polarizability, optical basicity and non-linear optical properties of oxide glasses, J. Non Cryst. Solids 249 (1999) 160–179, https://doi.org/10.1016/S0022-3093(99)00317-8.
[44] A.A. Abuelwafa, R.M. Matiur, A.A. Putri, T. Soga, Synthesis, structure, and optical properties of the nanocrystalline bismuth oxyiodide (BiOI) for optoelectronic application, Opt. Mater. (Amst.). 109 (2020) 1–10, https://doi.org/10.1016/j.optmat.2020.110413.
[45] M. Ezzeldien, H.Y. Morshidy, A.M. Al-boajan, A.M. Al Souwaileh, Z.A. Alrowaili, M.S. Sadeq, Environmental impacts of La2O3 on the optical and ligand field parameters of Ni ions inside Na2O-B2O3 glass, J. Alloy. Compd. 961 (2023), 170891, https://doi.org/10.1016/j.jallcom.2023.170891.
[46] T. Nishida, Advances in the Mössbauer effect for the structural study of glasses, J. Non Cryst. Solids 177 (1994) 257–268, https://doi.org/10.1016/0022-3093(94)90539-8.
[47] N. Mary, M. Rebours, E. Castel, S. Vaishnav, W. Deng, A.M.T. Bell, F. Clegg, B. L. Allsopp, A. Scrimshire, P.A. Bingham, Enhanced thermal stability of high-bismuth borate glasses by addition of iron, J. Non Cryst. Solids 500 (2018) 149–157, https://doi.org/10.1016/j.jnoncrysol.2018.07.061.
[48] P.A. Bingham, J.M. Parker, T. Searle, J.M. Williams, I. Smith, Novel structural behaviour of iron in alkali-alkaline-earth-silica glasses, Comptes Rendus Chim. 5 (2002) 787–796, https://doi.org/10.1016/S1631-0748(02)01444-3.
[49] E. Reguera, J.F. Bertran, J. Miranda, C. Portilla, Study of the dependence of Mössbauer parameters on the outer cation in nitroprussides, J. Radioanal. Nucl. Chem. Lett. 165 (1992) 191–201, https://doi.org/10.1007/BF02172242.
[50] L.H. Ahrens, Anion affinity and polarizing power of cations, Nature 169 (1952) 463, https://doi.org/10.1038/169463a0.
[51] D.F.V. Lewis, M. Dobrota, M.G. Taylor, D.V. Parke, Metal toxicity in two rodent species and redox potential: evaluation of quantitative structure-activity relationships, Environ. Toxicol. Chem. 18 (1999) 2199–2204, https://doi.org/10.1897/1551-5028(1999)018<2199:MTITRS>2.3.CO;2.